Geochemical Perspectives Letters

Fast REE re-distribution in mantle clinopyroxene *via* reactive melt infiltration

G. Borghini, P. Fumagalli, F. Arrigoni, E. Rampone, J. Berndt, S. Klemme, M. Tiepolo

Supplementary Information

The Supplementary Information includes:

- Experimental Procedure
- Analytical Techniques
- Tables S-1 to S-10
- Figures S-1 to S-3
- Supplementary Information References

Experimental Procedure

Experiments were performed at 1, 1.5 and 2 GPa on homogeneous mixtures of glass and minerals. Selected tholeiitic basaltic glass from Romanche Fracture Zone is moderately evolved (X_{Mg} = 0.60, $Na_2O + K_2O$ = 4.29 wt. % and displays Enriched-MORB (E-MORB)-like trace element signatures (La_N/Sm_N = 1.90, Sm_N/Yb_N = 2.71; data normalised to chondrite; Anders and Grevesse, 1989; Fig. S-1, Table S-1). We used a simplified mantle assemblage made by olivine and clinopyroxene in order to enhance the growth of clinopyroxene rims large enough to be analysed by laser ablation ICP-MS techniques.

The mantle peridotite component is simulated by mixing in equal proportions San Carlos olivine (Fo_{90}) and clinopyroxene separated from a fertile lherzolite from Northern Apennine ophiolitic sequences (BG6 sample, Borghini *et al.*, 2011). The clinopyroxene grains consist of spinel-facies porphyroclasts that contain very thin (2–10 μm) orthopyroxene exsolutions. Average clinopyroxene composition is X_{Mg} of 0.90 with moderate Al, high Ca and low Na (Al_2O_3 = 7.53 wt. %, CaO = 21.87 wt. %, Na_2O = 0.81 wt. %; Table S-1). The trace element composition is characterised by a slightly depleted LREE pattern (La_N/Sm_N = 0.23) and nearly flat MREE-HREE patterns at about 10× CI (Fig. S-1), which is typical of clinopyroxenes in equilibrium with Normal (N-) MORB (*e.g.*, Hofmann, 1988; Gale *et al.*, 2013). San Carlos olivine and BG6 clinopyroxene crystals were crushed in a boron carbide mortar and then sieved, selecting the olivine grains <63 μm and clinopyroxene crystals between 160 and 250 μm in size. We used a larger grain size of initial clinopyroxene to evaluate the rate of clinopyroxene textural replacement by the reaction with the melt as a function of experimental temperature and run duration. The basaltic glass was leached to remove potential sea-water-related contamination: glass chips were crushed, then placed in a beaker, covered by 8 N HNO_3 and then placed in a ultrasonic bath for 10 minutes. The leached glass was dried in oven at 60 °C for a minimum of two hours and crushed in ethanol in an agate mortar. The weighting procedure of starting materials mixing was carried out with a precision balance to five decimal places. We prepared two starting material mixtures with proportions of 1:1:1 and 2:1:1 of basalt:clinopyroxene:olivine, respectively, in order to investigate the effect of two initial

melt/peridotite ratios. Experiments were carried out using the "rocking" end-loaded piston cylinder at the Laboratorio di Petrologia Sperimentale, Dipartimento di Scienze della Terra "A. Desio", University of Milan, using talc-pyrex-MgO piston cylinder assemblies. A pressure correction for friction of 10 % was experimentally calibrated using the quartz-coesite transition (Bohlen and Boettcher, 1982). A graphite inner capsule granted the chemical isolation of the sample from the outer Pt-capsule thus minimising the Fe loss, and it also maintained the oxygen fugacity of the experiments below the graphite–CO buffer (*e.g.*, Ulmer and Luth, 1991; Medard *et al.*, 2008). To ensure nominally anhydrous conditions, the graphite lined Pt-capsule with the starting material was dried in oven at 250 °C for a minimum of three hours, before it was welded shut. Temperatures were measured with type S thermocouples (with an accuracy of ±5 °C) that were separated from the Pt capsule by a 0.6-mm thick hard alumina disc. According to piston cylinder calibration, pressure uncertainties are within ±3 %. We terminated the runs by turning off the electrical power, which resulted in initial quench rates of about 90 °C/sec. Capsules were cleaned with an abrasive tip, enclosed in epoxy, sectioned lengthwise and polished with diamond paste.

Analytical Techniques

Major elements microanalyses were performed using a JEOL JXA 8200 Superprobe at the Dipartimento di Scienze della Terra "Ardito Desio", University of Milan. Analyses on experimental minerals were acquired using 1 µm beam size, with an acceleration voltage of 15 kV and a beam current of 15 nA. Typical acquisition time was 30 s counting on peaks and 10 s counting on the background. In order to prevent alkali loss, we analysed glass using a beam size of 5 µm.

X-ray maps allowed image analysis using the *Fiji Image* processing package of *ImageJ software* (Rueden *et al*., 2017), which provided reliable estimates of modal abundances after the reaction experiments. Trace elements of the experimental run products were measured in two independent laboratories. Trace element concentrations in the experiment run products were determined by laser ablation inductively coupled plasma mass spectrometry (LA-ICP-MS) analyses at the Institute for Mineralogy, Universität Münster. Ablation of target materials was performed using a pulsed 193 nm ArF excimer laser (Analyte G2, Photon Machines), with a repetition rate of 10 Hz and an energy of ~3–4 J/cm^2. Depending on the dimensions of the target material, beam diameters were varied between 10 and 65 µm. The following isotopes were measured: ^{7}Li, ^{11}B, ^{29}Si, ^{43}Ca, ^{49}Ti, ^{51}V, ^{53}Cr, ^{55}Mn, 59Co, ^{60}Ni, ^{63}Cu, ^{66}Zn, ^{69}Ga, ^{73}Ge, ^{85}Rb, ^{88}Sr, ^{89}Y, ^{90}Zr, ^{93}Nb, ^{95}Mo, ^{133}Cs, ^{137}Ba, ^{139}La, ^{140}Ce, ^{141}Pr, ^{146}Nd, ^{147}Sm, ^{153}Eu, ^{157}Gd, ^{159}Tb, ^{163}Dy, ^{165}Ho, ^{166}Er, ^{169}Tm, ^{172}Yb, ^{175}Lu, ^{178}Hf, ^{181}Ta, ^{182}W, ^{208}Pb, ^{232}Th and ^{238}U. The analyses were calibrated using the NIST 610 glass reference material as a primary standard, with standard measurements acquired after approximately every 20 samples analyses. Additional measurements were made of the NIST 612 glass, as well as the USGS BIR-1G and BHVO-2G glass reference materials. Internal standards for the analyses were Si and Ca, obtained from the EMPA dataset and (in the case of the reference materials) the GeoReM database (Jochum *et al.*, 2011). Averages of all the NIST 610 glass measurements were within 2 % of the GeoReM values for all elements. Percent relative standard deviation (% r.s.d.) values for the NIST 610 glass measurements were less than 5 % for most elements and typically less than 2 % for the larger, 40–65 µm spots. The % r.s.d. values for repeat measurements of the NIST 612, BIR-1G and BHVO-2G glasses are typically 10–25 % (Table S-10a), and lower than 10 % on average for the 40–65 µm spot diameters. The data were reduced using the GEMOC GLITTER software (Griffin *et al.*, 2008), including monitoring the signal selection to identify and exclude any instances where the beam may have hit inclusions or grain boundaries.

Trace elements concentrations in minerals and glasses were determined with LA-ICP-MS at the Geochemistry, Geochronology and Isotope Geology laboratory of Dipartimento di Scienze della Terra "Ardito Desio", University of Milan. The instrument couples an ArF 193 nm excimer laser microprobe, equipped with HelEx II volume sample chamber (Analyte Excite - Teledyne CETAC), with a quadrupole ICP-MS system (iCAP-RQ Thermo Scientific). Laser spot diameter ranges from 25 to 40 µm as a function of the mineral/glass dimensions. The laser fluence was 2.5 J/cm^2 for glass and clinopyroxene. The laser repetition rate was set to 10 Hz for all minerals. The He flow rate was set to 0.5 L/min and to 0.2 L/min into the sample chamber and in the HelEx II cup, respectively. NIST-612 was used as an external standard, whereas ^{43}Ca and ^{29}Si were adopted as internal standards, depending on the analysed material. Each analysis consisted in the acquisition of a total of 120 s that included 40 s of background signal (comprising 10 s

of laser warm up), about 60 s of laser signal followed by 20 s of wash out time. Quality control was achieved analysing in each analytical run the USGS reference basalt glasses BCR- 2G as unknown. Precision is better than 10 % and accuracy is within 2σ of the preferred values (Table S-10b). Data reduction was carried out using the Glitter software package (Griffin *et al.*, 2008).

EBS images coupled to X-ray maps oriented us in the localisation of ideal microstructural sites where performing laser ablation analyses and this was applied in particular for the analyses on the reaction rims of clinopyroxene. However, despite of development of rather coarse texture in experimental sample, some clinopyroxene analyses likely suffered from the contamination by interstitial glass that resulted in artificial very intense LREE enrichment. In order to avoid such contamination, we filtered trace element data based on the Ba content, *i.e.* selecting analyses with Ba > 1 ppm in agreement with the very low distribution coefficient of Ba between clinopyroxene and silicate melts (*e.g.*, Hart and Dunn, 1993; Ma and Shaw, 2021).

Supplementary Tables

Table S-1 Major (wt. %) and trace (ppm) element compositions of starting materials.

Table S-2 Experimental conditions and run products.

Table S-3 Major element compositions (wt. %) of olivines in reaction experiments.

Table S-4 Major element compositions (wt. %) of new clinopyroxenes in reaction experiments.

Table S-5 Major element compositions (wt. %) of relict clinopyroxenes in reaction experiments.

Table S-6 Major element compositions (wt. %) of reacted glasses in reaction experiments.

Table S-7 Major element compositions (wt. %) of glass and clinopyroxene in crystallisation experiments at 2 GPa and 1300 °C.

Table S-8 Trace element concentrations (ppm) in clinopyroxenes.

Table S-9 Trace element concentrations (ppm) in glasses.

Table S-10 Trace element compositions of standards measured during LA-ICP-MS analyses.

Tables S-1 to S-10 (.xlsx) are available for download from the online version of this article at https://doi.org/10.7185/geochemlet.2323.

Supplementary Figures

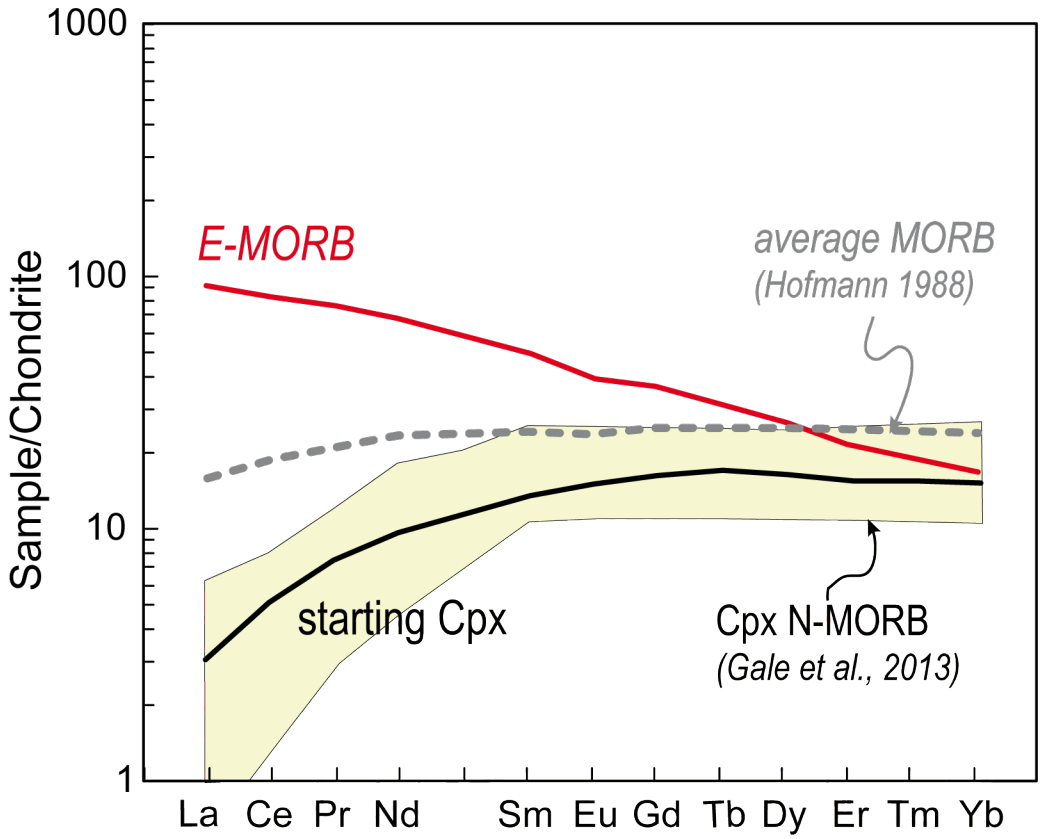

Figure S-1 Chondrite normalised REE patterns of initial clinopyroxene and E-MORB glass used in reaction experiments (from Table S-1). Also reported are the average REE composition of MORB (Hofmann, 1988) and the field defined by computed REE patterns of clinopyroxenes in equilibrium with N-MORB from Gale *et al.* (2013).

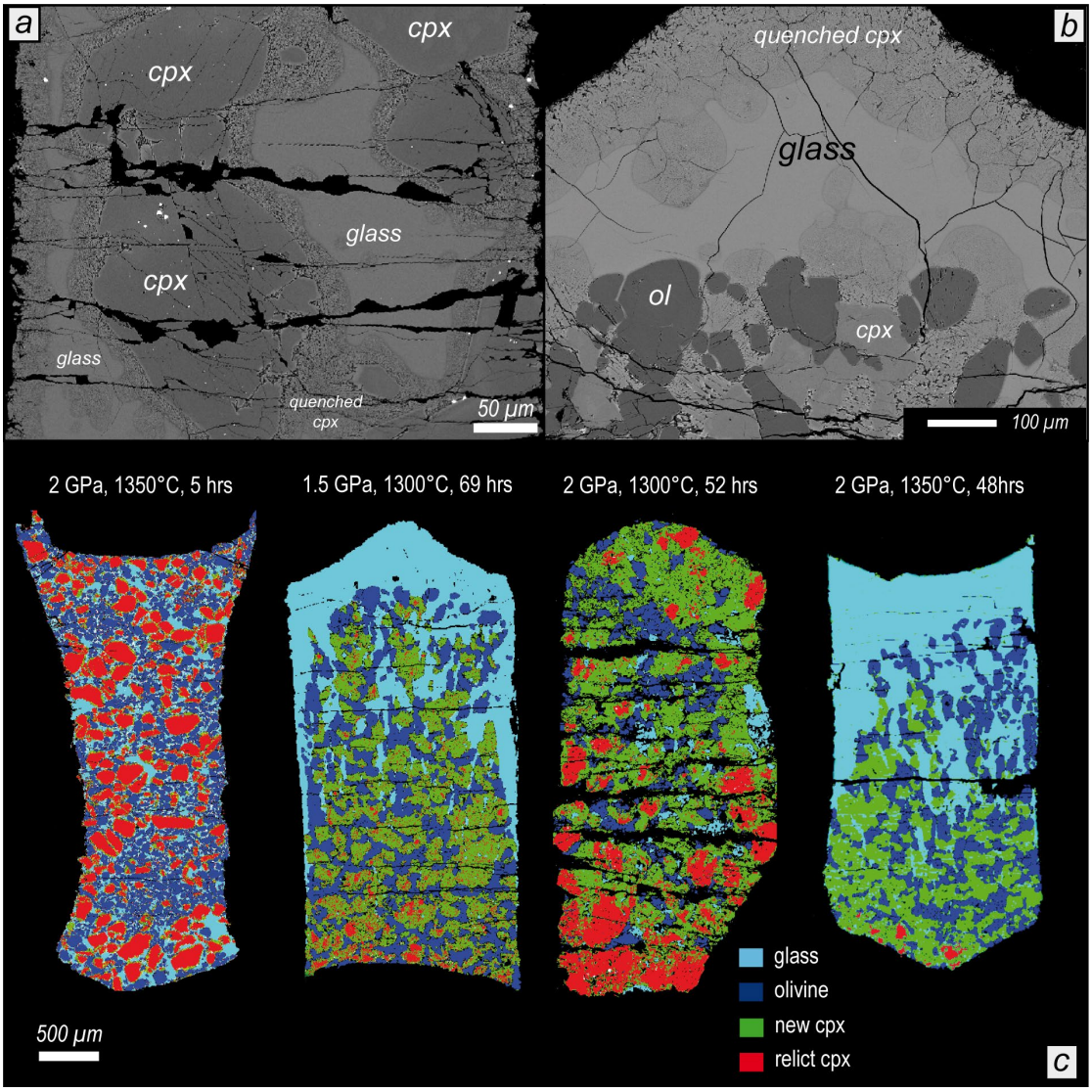

Figure S-2 **(a)** Backscattered electron (BSE) image showing large clinopyroxene grains coexisting with glass in crystallisation experiments at 2 GPa, 1300 °C; the growth of chemically homogeneous, unzoned clinopyroxene grains and mass balance calculation with very low sum of the squares of the residuals (R^2 = 0.1123; 0.19 cpx and 0.81 glass), strongly support the attainemnt of equilibrium in this crystallisation run. **(b)** Run products of reaction experiment at 1.5 GPa and 1300 °C, consisting of rounded olivine, prismatic clinopyroxene and glass. Olivine has straight boundary against glass and clinopyroxene suggesting it requilibrated with reacted glass and new clinopyroxe. No unreacted olivine is identifiable because it always it has homogeneous composition, significantly different from starting SC olivine, as observed in dunite-basalt reaction experiments (Borghini *et al.*, 2018, 2022). Accumulation of reacted glass at the top of experimental charge favored the in situ measurements of trace element concentrations. **(c)** Phase maps derived by combining X-ray concentration maps (Ca, Mg, Al) of reaction experiments at 1.5 and 2 GPa on starting material with basalt:clinopyroxene:olivine weight proportions of 1:1:1. Image analyses revealed that experiment at 2 GPa and 1300 °C experienced high extent of reacted glass crystallisation.

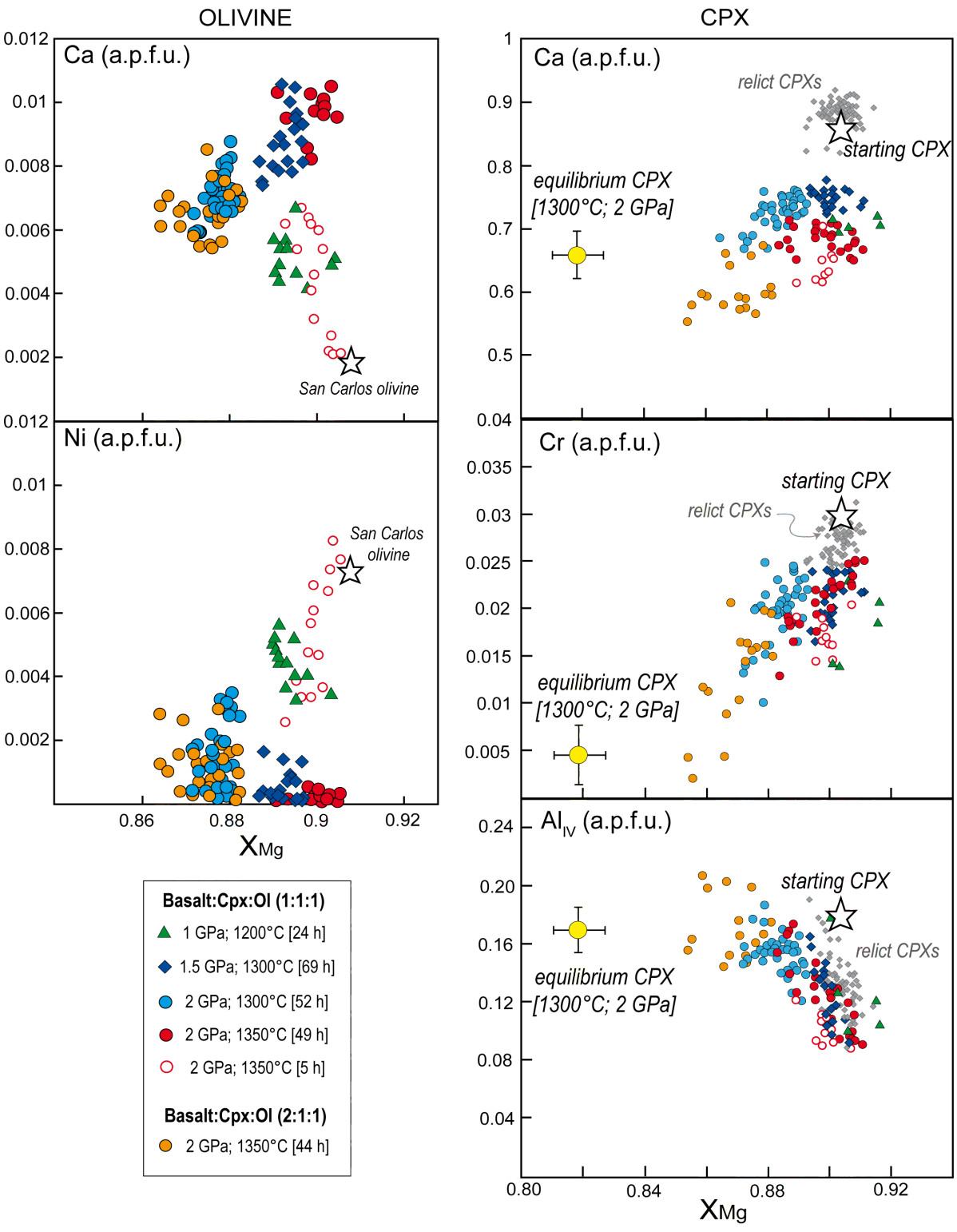

Figure S-3 Major element compositions of olivine (X_{Mg} *versus* Ca and Ni a.p.f.u.) and clinopyroxene (X_{Mg} *versus* Ca, Na and Al_{IV} a.p.f.u.) from crystallisation and reaction experiments. Composition of starting olivine and clinopyroxene are reported for comparison.

Supplementary Information References

Anders, E., Grevesse, N. (1989) Abundances of the elements: meteoric and solar: *Geochimica et Cosmochimica Acta* 53, 197–214. https://doi.org/10.1016/0016-7037(89)90286-X

Bohlen, S.R., Boettcher, A.L. (1982) The quartz -coesite transformation: a precise determination and the effects of other components. *Journal of Geophysical Research* 87, 7073–7078. https://doi.org/10.1029/JB087iB08p07073

Borghini, G., Fumagalli, P., Rampone, E. (2011) The geobarometric significance of plagioclase in mantle peridotites: A link between nature and experiments. *Lithos* 126, 42–53. https://doi.org/10.1016/j.lithos.2011.05.012

Borghini, G., Rampone, E., Zanetti, A., Class, C., Cipriani, A., Hofmann, A. W., Goldstein, S. L. (2016) Pyroxenite layersin the Northern Apennines upper mantle (Italy) – Generation by pyroxenite melting and melt infiltration. *Journal of Petrology* 57, 625–653. https://doi.org/10.1093/petrology/egv074

Borghini, G., Fumagalli P., Francomme J.E. (2018) Melt-dunite interactions at 0.5 and 0.7 GPa: experimental constraints on the origin of olivine-rich troctolites. *Lithos* 323, 44–57. https://doi.org/10.1016/j.lithos.2018.09.022

Borghini, G., Fumagalli, P., Rampone, E. (2022) Melt-rock interactions in a veined mantle: pyroxenite-peridotite reaction experiments at 2 GPa. *European Journal of Mineralogy* 34, 109–129. https://doi.org/10.5194/ejm-34-109-2022

Gale, A., Dalton, C.A., Langmuir, C.H., Su, Y., Schilling, J.G. (2013) The mean composition of ocean ridge basalts. *Geochemistry Geophysics Geosystems* 14, 489–518. https://doi.org/10.1029/2012GC004334

Griffin, W.L., Powell, W., Pearson, N.J., O'Reilly, S.Y. (2008) GLITTER: data reduction software for laser ablation ICP-MS. In Sylvester, P. (ed.), Laser Ablation ICP-MS in the Earth Sciences: Current practices and outstanding issues: Mineralogical Association of Canada, Short Course Series, 40, p. 307-311.

Hart, S.R., Dunn, T. (1993) Experimental cpx/melt partitioning of twenty-four trace elements. *Contributions to Mineralogy and Petrology* 113, 1–8. https://doi.org/10.1007/BF00320827

Hofmann, A.W. (1988) Chemical differentiation of the earth: the relationships between mantle, continental crust and oceanic crust. *Earth and Planetary Science Letters* 90, 297–314. http://dx.doi.org/10.1016/0012-821X(88)90132-X

Jochum, K.P., Wang, X., Nohl, U., Schmidt, S., Schwager, B., Stoll, B., Yang, Q., Weis, U. (2011) Geostandards and geoanalytical research bibliographic review 2010. *Geostandards and Geoanalytical Research* 35, 485–488. https://doi.org/10.1111/j.1751-908X.2011.00164.x

Ma, S., Shaw, C.S.J. (2021) An experimental study of trace element partitioning between peridotite minerals and alkaline basaltic melts at 1250°C and 1 GPa: crystal and melt composition impacts on partition coefficients. *Journal of Petrology* 62, 1–27. https://doi.org/10.1093/petrology/egab084

Médard, E., McCammon, C.A., Barr, J.A., Grove, T.L. (2008) Oxygen fugacity, temperature reproducibility, and H_2O contents of nominally anhydrous piston-cylinder experiments using graphite capsules. *American Mineralogist* 93, 1838–1844. https://doi.org/10.2138/am.2008.2842

Rueden, C.T., Schindelin, J., Hiner, M.C., DeZonia, B.E., Walter, A.E., Arena, E.T., Eliceiri, K.W. (2017) ImageJ2: ImageJ for the next generation of scientific image data. *BMC Bioinformatics*, 18, 529. https://doi.org/10.1186/s12859-017-1934-z

Ulmer, P., Luth, R.W. (1991) The graphite fluid equilibrium in P, T, fO_2 space: an experimental determination to 30 kbar and 1600°C. *Contributions to Mineralogy and Petrology* 106, 265–272. https://doi.org/10.1007/BF00324556